Efficient Single-Photon Sources Based on Low-Density Quantum Dots in Photonic-Crystal Nanocavities

Wen-Hao Chang,[1] Wen-Yen Chen,[1] Hsiang-Szu Chang,[1] Tung-Po Hsieh,[2] Jen-Inn Chyi,[2] and Tzu-Min Hsu[1,*]
[1]*Department of Physics, National Central University, Chung-li, 32054 Taiwan, Republic of China*
[2]*Department of Electrical Engineering, National Central University, Chung-li, 32054 Taiwan, Republic of China*
(Received 21 September 2005; published 20 March 2006)

An efficient single-photon source based on low-density InGaAs quantum dots in a photonic-crystal nanocavity is demonstrated. The single-photon source features the effects of a photonic band gap, yielding a *single-mode* spontaneous emission coupling efficiency as high as $\beta = 92\%$ and a linear polarization degree up to $p = 95\%$. This appealing performance makes it well suited for practical implementation of polarization-encoded schemes in quantum cryptography.

DOI: 10.1103/PhysRevLett.96.117401 PACS numbers: 78.67.Hc, 42.50.Dv, 42.50.Pq, 42.70.Qs

A deterministic source of single photons is a crucial prerequisite for the implementation of quantum information processing [1], particularly for quantum cryptography [2]. Single semiconductor quantum dots (QDs) are excellent candidates of stable, solid-state emitters for such applications [3–7]. Initial concerns of low photon extraction efficiency caused by the high-refractive-index surrounding have been dispelled by incorporating QDs into a solid-state, monolithic microcavity [3–5]. Such approaches exploit the Purcell effect [8], or the cavity quantum electrodynamics (cavity QED) in the weak coupling regime, to enhance the spontaneous emission (SE) rate into a specific cavity mode and, thereby, achieve fast, efficient, or even directional single-photon emissions. Over the past few years, this idea has been implemented using microdisk [3] and micropost [4,5] cavities with embedded QDs to demonstrate on-demand single-photon emissions.

Recently, focused attention was directed to nanocavities based on photonic-crystal (PC) structures [9]. Besides the capability of offering high quality factor (Q) and ultrasmall modal volume (V_m), the inherent flexibility and diversity in cavity design makes a PC nanocavity more promising in the tailoring of cavity-mode wavelength, polarization, and directionality through fine adjustments in lattice structures [10,11]. PC structures also promise to fully control (enhance or inhibit) the SE dynamics, through the modification of available optical modes by the PC surrounding [12]. Accordingly, a high SE coupling efficiency (β factor) is expected. This effect has recently been studied for an InGaAs QD ensemble [13] and individual dots [14] in a two-dimensional (2D) PC defect cavity. However, due possibly to the high-density QDs ($\sim 200/\mu\mathrm{m}^2$) used in these studies, different few-particle exciton states of individual QDs were not resolved and identified. Therefore, it is less clear whether other effects (e.g., multiexciton lines, background emissions, and/or interdot energy transfer effects [15,16]) contribute to the observed changes in SE decay rates in such high-density QDs. Moreover, high-density QDs also significantly limit the performance of single-photon emission, due to the coupling of many QDs into the cavity mode, yielding undesired multiphoton emissions especially when higher injection rates were used.

In this Letter, we report an efficient single-photon source based on low-density InGaAs QDs ($\sim 3/\mu\mathrm{m}^2$) in 2D PC structures with defect-type nanocavities. Since each cavity contains only 1–2 dots, the few-particle exciton lines of both on- and off-resonance QDs are well resolved; hence, the cavity-QED effects for both cases are unambiguously demonstrated. We utilize a linear-type PC nanocavity to couple single QD emissions, so that the generated single photons can be coupled into a single *nondegenerate* cavity mode with a well defined polarization state. A very high single-mode SE coupling efficiency and a very large degree of linear polarization have been achieved, making the single-photon source well suited for practical applications.

The sample was grown on a GaAs substrate by low-pressure metalorganic chemical vapor deposition. A layer of self-assembled $In_{0.5}Ga_{0.5}As$ QDs was inserted into the center of a 180-nm GaAs layer grown on a 500-nm $Al_{0.8}Ga_{0.2}As$ layer. To ensure isolated QD emissions, the QD density was reduced to $\sim 3/\mu\mathrm{m}^2$ through careful control of InGaAs coverage [17]. PC structures consisting of 2D triangular lattices of air holes were fabricated into the GaAs layer by electron-beam lithography and dry etching. The underneath $Al_{0.8}Ga_{0.2}As$ layer was finally removed by selective wet etching, forming a suspended PC membrane. The PC structures have an air-hole periodicity of $a = 300$ nm and radius of $r = 0.31a$. In this structure, a photonic band gap (PBG) is open only for a transverse-electric mode in the frequency range of 0.25–0.33(c/a), corresponding to a wavelength range of 0.9–1.2 μm. A nanocavity was formed by introducing three missing air holes in a line [see Fig. 1(a)], i.e., the so-called L3 defect [11,18] in 2D triangular PC lattices. The two air holes at both edges were displaced outward by a shift s varied systematically from 0 to $0.25a$.

Optical emissions were characterized by microphotoluminescence (μPL) at 5–8 K using a He-Ne laser (633 nm)

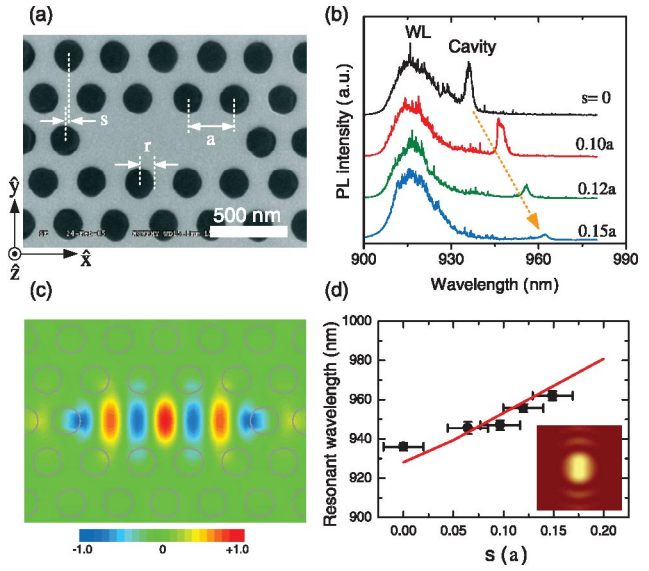

FIG. 1 (color). (a) Scanning electron micrograph of the fabricated nanocavity with $a = 300$ nm, $r = 0.31a$, and $s = 0.1a$. (b) μPL spectra for a series of nanocavities with $s = 0$–$0.15a$ under $P_{ex} \sim 5$ kW/cm^2. (c) The calculated electric field profile (E_y) of the shallow donor-type cavity mode confined in the L3-defect cavity with $s = 0.1a$. The color scale is normalized to max($|E_y|$). (d) The calculated (solid line) and the measured (solid squares) resonant wavelengths of the cavity mode as a function of s. The inset in (d) shows the calculated far-field radiation pattern of the cavity mode.

focused onto the cavity region via an objective lens (N.A. = 0.65). The cavity emission was collected by the same objective lens and analyzed by a 0.64-m triple monochromator. Because of the low QD density, cavity-mode structures were investigated under high excitation conditions (~ 5 kW/cm^2). The resulting spectra are shown in Fig. 1(b). The wetting-layer (WL) emission band was observed near 915 nm. Cavity-mode resonance was found at the long-wavelength side of the WL emission. These cavity modes were highly reproducible for nominally the same cavity. As s varying from 0 to $0.15a$, the resonant wavelength shifts systematically from 938 to 962 nm. This redshift manifests itself as a cavity-mode resonance rather than resonances at PBG edges. To further analyze the cavity mode, the cavity structures have been studied using three-dimensional (3D) finite-difference time-domain (FDTD) calculations. We identified the observed cavity mode as a shallow donor-type defect mode. The calculated electric field profile (E_y) of this mode is well localized in the defect region [Fig. 1(c)] with $V_m \approx 0.7(\lambda/n)^3$. This cavity mode is resonating predominantly along $\hat{x}$ axis, so that increasing s effectively increases the "cavity length," yielding a longer resonant wavelength. In Fig. 1(d), the measured resonant wavelength as a function of s follows this trend and quantitatively agrees with our FDTD calculations. We have also studied the far-field radiation pattern of the cavity mode. The calculated vertical component of the Poynting vector is concentrated [inset in Fig. 1(d)], which can be efficiently collected by an objective lens and facilitates outcoupling into downstream components. We also noted that the calculated vertical radiation carries a predominant E_y component; namely, the radiation from the cavity mode is y-polarized. Polarization measurements of the cavity emission also show a strong linear polarization along the $\hat{y}$ axis, matching perfectly with the 3D-FDTD calculations and confirming this mode assignment.

Individual QD emissions can be resolved under lower excitation conditions. Figure 2(a) shows the μPL spectra obtained from one of the fabricated nanocavities as a function of excitation power P_{ex}. According to the QD density, each cavity would contain only 1–2 dots. We select in Fig. 2(a) a cavity displaying two sets of lines, corresponding to emissions from two different single QDs (labeled QD1 and QD2), to highlight the different behaviors of QDs on resonance and off resonance with the cavity mode. For QD1, the emission lines at 942.4 and 944.0 nm were identified as single-exciton (X) and biexciton ($2X$) lines, according to their linear and quadratic power dependence of intensity [Fig. 2(b)], respectively. A similar behavior was also observed for QD2, of which single-exciton (X') and biexciton ($2X'$) lines show similar power dependence, except a much weaker intensity and a several times lower saturation power for the X' line. This striking difference implicates that QD1 is on resonance with the cavity mode, while QD2 is out of resonance. Indeed, the cavity-

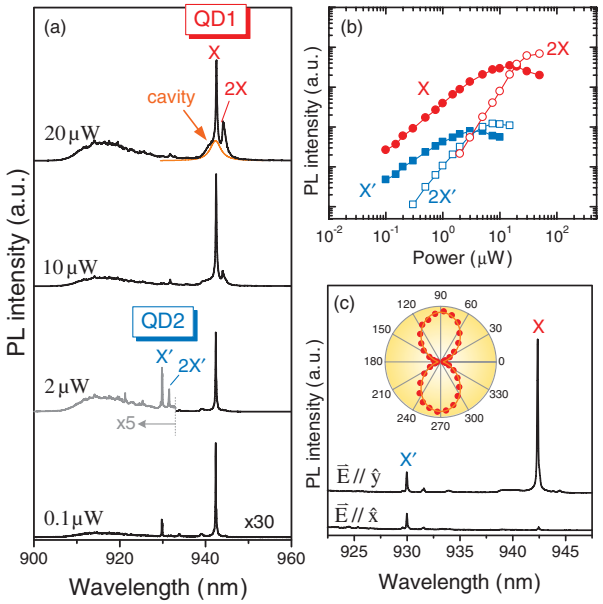

FIG. 2 (color). (a) μPL spectra obtained from one of the fabricated nanocavity with $s = 0.1a$ under different P_{ex}. (b) The intensities of exciton and biexciton lines of two different QDs as a function of P_{ex}. (c) Polarization-resolved spectra with electric field $\vec{E}$ parallel to the $\hat{x}$ and $\hat{y}$ directions. The inset shows a polar plot of the X-line intensity as a function of polarization angle.

mode structure is visible under higher P_{ex}'s and matches spectrally with the X line. We estimated $Q \sim 300$ for this mode and a wavelength detuning of ~0.1 nm from the X line according to multiple Lorentzian fittings. The QD-cavity coupling can be further confirmed by examining the polarization of these emission lines [Fig. 2(c)]. Since the exciton line of uncoupled QDs shows no preferential polarization (due possibly to the small fine-structure splitting) [19], emission lines with polarization matched with that of the cavity mode can be direct evidence for the QD-cavity coupling. As shown in Fig. 2(c), the X line of QD1 is strongly y-polarized with a polarization degree $p(\equiv |I_x - I_y|/|I_x + I_y|) = 95\%$, manifesting the QD-cavity coupling of QD1.

To explore the cavity-QED effects, we investigated the SE dynamics of single QDs by time-resolved μPL. In this experiment, the sample was excited by 200-fs pulses at 1.55 eV from a Ti:sapphire laser. The resulting temporal decay traces were detected by a Si-avalanche photodiode (APD) and time-correlated photon counting electronics, having an overall temporal resolution of ~150 ps after applying deconvolution technique. The intrinsic lifetime τ_0 for QDs without the PC effects was determined to be $\tau_0 = 0.65(\pm 0.05)$ ns by investigating nearly 20 QDs of similar emission wavelength. With the PC nanocavity, dramatic modifications in SE lifetimes were observed [Fig. 3]. For the X line of QD1 on resonance with the cavity mode, the SE lifetime is shortened to $\tau_1 = 0.21$ ns, corresponding to a threefold ($\tau_0/\tau_1 \approx 3$) enhanced SE rate due to the Purcell effect. This threefold enhancement can be compared with the Purcell factor $F_P = 3Q(\lambda/n)^3/4\pi^2 V_m$. For the nanocavity discussed here, the simulated $V_m \approx 0.7(\lambda/n)^3$ together with $Q \sim 300$ determine $F_P = 38$. This figure of merit was usually deteriorated due to a number of factors, including misalignments of QD spectral positions, spatial locations, and polarization orientations with the cavity mode [20]. For the off-resonance QD2, by contrast, a much longer lifetime of $\tau_2 = 2.52$ ns was observed for the X' line, corresponding to a fourfold ($\tau_0/\tau_2 \approx 1/4$) suppressed SE rate. The enhanced and inhibited SE rates reported here represent a experimental demonstration of a full control of the SE dynamics of *single* QDs by the PC nanocavities. We point out that the interdot energy transfer effect [15] due to the dipole-dipole interaction, which may be more relevant in high-density QDs, can be ruled out from the observed modifications in SE rates for such low-density QDs. In fact, we also found that the emitted photons from different QDs are uncorrelated [16] (i.e., no interdot exciton transfer), further confirming that the changes in SE rates are indeed arisen from the cavity-QED effect.

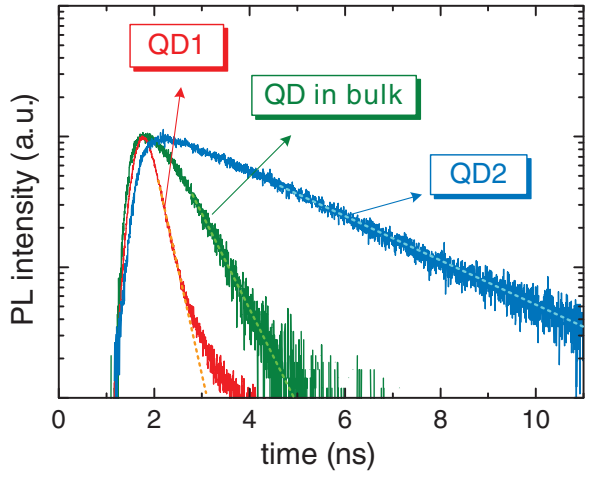

FIG. 3 (color). Time-resolved μPL traces of the QDs on resonance (QD1), off resonance (QD2), and in bulk without the PC effects.

The measured lifetimes for QDs on and off resonance can be utilized to estimate SE coupling efficiency, i.e., the β factor, defined as the fraction of emitted photons being captured into a single cavity mode [13,14,21]. It can be expressed as $\beta = (\gamma - \gamma_{PC})/\gamma$, where the total SE rate γ is view as the sum of rates into cavity mode γ_C and into the PC surrounding γ_{PC} (i.e.,$\gamma = \gamma_C + \gamma_{PC}$). If we assume $\gamma_{PC} \approx 1/\tau_2$, the single-mode coupling efficiency would be $\beta \approx 1 - (\tau_1/\tau_2) = 92\%$. Such a high β factor highlights the importance of the use of a PC nanocavity. Radiations leaked into the PC surrounding were eliminated due to the diminished optical states in the 2D PBG. Consequently, the emitted photons were predominantly funneled into the cavity mode, despite the moderate cavity Q, because of the inhibited γ_{PC}. This is in striking contrast to other solid-state cavities [21], in which a high β relies mainly on enhanced γ_C by a larger Purcell enhancement.

Triggered single-photon generations were achieved by pulsed excitation on the QDs in PC nanocavities. The emitted photons were first spectrally filtered and then directed towards a Hanbury-Brown–Twiss– (HBT-) type setup [22] to characterize the performance of the single-photon source. The resulting histograms, which represent the second order correlation function $g^{(2)}(\tau)$, are shown in Fig. 4. For the spectrally filtered X line of QD1, the measured histogram [Fig. 4(a)] shows a reduced peak area at $\tau = 0$, i.e., a clear signature of photon antibunching. These coincident peaks are narrow, almost limited by the time resolution of our HBT setup, implicating a single-photon source with low timing jitters owing to the cavity-enhanced SE rate. The nonzero $g^{(2)}(0) \leq 0.2$ most likely arise from the coupling of background emissions (e.g., WL) into the cavity mode. If we take into account the known background level according to spectral measurements, the actual probability of multiphoton emission would be $g^{(2)}(0) \approx 0.05$. The remainder may be due to the refilling of carriers from the GaAs barrier or the WL into the QD after emission of a first photon. This effect is particularly relevant when the radiative lifetime in QDs is

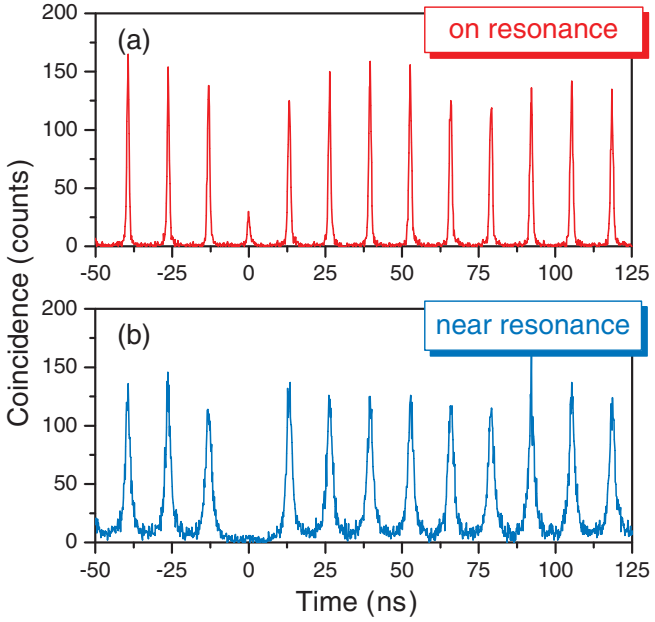

FIG. 4 (color). (a) The measured photon correlation histogram of the spectrally filtered X line of the on-resonance QD1 under pulsed excitation. (b) The histogram obtained from another QD in another cavity with nominally the same PC structures but with a larger detuning. The excitation energy, the pumping power, and the repetition rate in both cases are 1.55 eV, 2 μW, and 76 MHz, respectively.

considerably shortened by the Purcell effect and becomes comparable to the carrier lifetime in the GaAs and the WL. Using a resonant excitation scheme may mitigate the impact of this effect [23]. We have also investigated another single QD in another cavity with nominally the same PC structure but with a larger detuning and, hence, a longer emission lifetime (1.2 ns). In this case, the multiphoton event was further reduced to $g^{(2)}(0) \leq 0.01$ [Fig. 4(b)], corresponding to a hundredfold suppressed multiphoton emission as compared with a Poissonian source. This implies that using a near-resonance QD can eliminate the background level considerably, however, at the expense of larger timing jitters due to the relatively longer emission lifetime.

We have also estimated the collection efficiency according to the measured photon counting rate from the APD under pulsed excitations. After considering all optics and components used in our systems, the collection efficiency for the PC-based single-photon source is estimated to be around 10%–20%, which is at least 1–2 orders of magnitude higher than those QDs without PC structure. However, we still lost at least half of the emitted photons, because only the upward emitting photons were collected. To achieve a higher external efficiency, the development of other outcoupling strategies (e.g., coupled cavity-waveguide structure) will be an important issue.

In summary, we demonstrate an efficient single-photon source based on low-density InGaAs QDs embedded in linear-type PC nanocavities. The few-particle exciton lines of both on- and off-resonance QDs are well resolved, and hence the cavity-QED effects for both cases are unambiguously demonstrated. Based on the effects of a PC cavity, we achieve *single-mode* operations for our single-photon source, which shows a high coupling efficiency, a high polarization degree, low multiphoton emission rates, as well as reduced timing jitters. This appealing performance makes it well suited for practical implementation of polarization-encoded schemes in quantum cryptography. The realization of PC-based quantum light sources also represents a crucial step toward the implementation of a prospective photonic integrated circuit for quantum networks.

This work is supported by the National Science Council of the Republic of China under Grant No. NSC-94-2120-M-008-001.

*Electronic address: tmhsu@phy.ncu.edu.tw

[1] E. Knill, R. Laflamme, and G. J. Milburn, Nature (London) **409**, 46 (2001).
[2] For a review, see, for example, N. Gisin *et al.*, Rev. Mod. Phys. **74**, 145 (2002).
[3] P. Michler *et al.*, Science **290**, 2282 (2000).
[4] E. Moreau *et al.*, Appl. Phys. Lett. **79**, 2865 (2001).
[5] M. Pelton *et al.*, Phys. Rev. Lett. **89**, 233602 (2002).
[6] C. Santori *et al.*, Phys. Rev. Lett. **86**, 1502 (2001).
[7] Z. Yuan *et al.*, Science **295**, 102 (2002).
[8] E. M. Purcell, Phys. Rev. **69**, 681 (1946).
[9] E. Yablonovitch, Phys. Rev. Lett. **58**, 2059 (1987).
[10] J. Vučković, and Y. Yamamoto, Appl. Phys. Lett. **82**, 2374 (2003).
[11] Y. Akahane *et al.*, Nature (London) **425**, 944 (2003); C. Sauvan, P. Lalanne, and J.-P. Hugonin, Nature (London) **429**, 10.1038/nature02602 (2004).
[12] P. Lodahl *et al.*, Nature (London) **430**, 654 (2004).
[13] A. Kress *et al.*, Phys. Rev. B **71**, 241304(R) (2005).
[14] D. Englund *et al.*, Phys. Rev. Lett. **95**, 013904 (2005).
[15] S. A. Crooker *et al.*, Phys. Rev. Lett. **89**, 186802 (2002).
[16] B. D. Gerardot *et al.*, Phys. Rev. Lett. **95**, 137403 (2005).
[17] T.-P. Hsieh *et al.*, Nanotechnology **17**, 512 (2006).
[18] Y. Akahane *et al.*, Appl. Phys. Lett. **82**, 1341 (2003).
[19] R. M. Stevenson *et al.*, Phys. Rev. B **66**, 081302(R) (2002).
[20] J.-M. Gérard *et al.*, Phys. Rev. Lett. **81**, 1110 (1998); J.-M. Gérard and B. Gayral, J. Lightwave Technol. **17**, 2089 (1999).
[21] G. S. Solomon, M. Pelton, and Y. Yamamoto, Phys. Rev. Lett. **86**, 3903 (2001).
[22] R. Hanbury Brown, and R. Q. Twiss, Nature (London) **178**, 1447 (1956).
[23] C. Santori *et al.*, New J. Phys. **6**, 89 (2004).